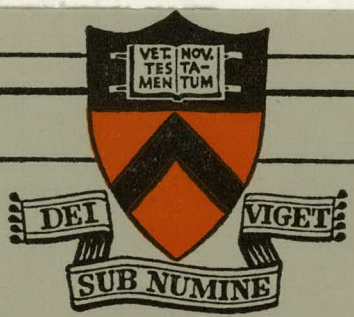

PRINCETON UNIVERSITY

DEPARTMENT OF AEROSPACE AND MECHANICAL SCIENCES

DISCLAIMER

First Semi-Annual Progress Report To The Sandia Corporation On AEC Sub-contract AT(30-1)-3451

On

THE COMBUSTION OF METALS

Sc-dc-65-1480

1 July 1964 to 31 December 1964

Prepared by:

James G. Hansel
Research Staff Member

Melvin Zwillenberg
Assistant-in-Research

Arthur M. Mellor
Assistant-in-Research

H. F. Sullivan
Fellow

Approved by:

Irvin Glassman
Professor
Principal Investigator

17 February 1965

Department of Aerospace & Mechanical Sciences
Guggenheim Laboratories for the Aerospace Propulsion Sciences
PRINCETON UNIVERSITY
Princeton, New Jersey

I. INTRODUCTION

This report is the first semi-annual progress report on AEC Sub-contract AT (30-1)-3451, covering the period 1 July 1964 to 31 December 1964. During this report period, the primary effort has been devoted to the construction of the necessary experimental apparatus as well as the performance of initial experiments with zirconium and tantalum. The development of an experimental method for measuring of metal flame temperature is also in progress. The ability to measure the metal flame temperature will inable the further verification of the criteria put forth by the Princeton group and will provide, as well, high temperature vapor pressure data of metal oxides such as aluminum oxide, strontium oxide, zirconium oxide, tantalum oxide, etc. Analytical and experimental work on the ignition of aluminum is reported as well. These researches are described in four sections which form the main body of the report.

It is felt that the time devoted to the construction and modification of the apparatus during this report period will permit the investigations outlined in the proposal to be carried out more effectively during the next report period.

I. The Ignition and Combustion of Tantalum in Oxygen

Preliminary experimental work has started on the ignition and combustion of tantalum wires in oxygen-argon mixtures. Work on calcium will proceed when pure specimens are available in near wire or wire form.

Tantalum wires of .030" diameter and 11 cm length were mounted in the electrodes in a L-shaped configuration as shown in Figure 1. The following photographs were taken through the window at the right center of Figure 1. The experiments to be described were performed in pure oxygen at pressures ranging from 50 mm Hg to 5 atm.

The sequence in the ignition and combustion of tantalum is as follows: as the wire is heated electrically, a uniform red glow progresses from the hottest protion of the wire, usually near the geometric center, towards the electrodes. A few seconds later, the hottest portion of the wire becomes white hot; this zone is considered to be the ignition zone and appears to consist of a solid-phase reaction. The wire then breaks near the center and apparently is consumed by a solid phase reaction as shown in Figure 2, which was photographed at 500mm Hg of oxygen. As shown, the flame is proceeding upwards. Note the ripples or waves feeding the molten ball of metal and oxide at the lower end of the wire. Occasionally, these molten balls fell to the bottom of the chamber.

If the combustion zone regressed as far as the electrode blocks, rather spectacular fragmentation was observed as the combustion zone was quenched and supercooled at the electrode. An example is shown in Figure 3, which was photographed at 5 atm of pure oxygen. The small particles given off appeared to continue to

burn.

In the pressure regime from 300 mm Hg to 1 atm, the samples at the electrodes then expanded and burst a few times, very similar to a child blowing a soap bubble.

As the oxygen pressure was increased, the duration of the reaction decreased.

The products of combustion most likely consist of Ta and Ta_2O_5 and assumed the shapes of hard glassy spheres and brittle flakes (which were formed when the molten balls quenched on the chamber bottom). White, brown, and black products were found together.

The vapor-phase combustion criterion, that the boiling point of the metal oxide be higher than the boiling point of the metal, cannot be checked readily for tantalum, as boiling point values for the oxide (Ta_2O_5) are not available. Wide discrepancies in the boiling point of the metal have been found, with values of 4100 (Ref. 1), 5430 (Ref. 2), and 6100°C (Ref. 3) given. However, from the experimental evidence discussed here, it appears that tantalum burns in the solid phase under the particular experimental conditions, which could be taken to indicate that the boiling point of the oxide is less than that of the metal.

During the next report period experiments on the ignition and combustion of tantalum will be continued, in mixtures of oxygen, nitrogen, carbon dioxide, water vapor, and argon. The possibilities of vapor phase flames in some pressure region will be examined carefully.

II. The Combustion of Zirconium in Oxygen and Oxygen-Argon Atmospheres

Zirconium wire samples .020" diameter and 11 cm. length have been ignited by resistance heating and burned in atmospheres of oxygen and oxygen-argon at various subatmospheric pressures. The wires are mounted in the electrodes horizontally. The voltage rise is linear with time.

As the wire is heated its surface passes through several color changes including blue, gold and purple. All of these color changes occur before the wire glows red hot. As heating continues, a hot spot occurs on the wire - as indicated in Figure 4 which is a photograph of a heated zirconium wire in pure oxygen at 50 mm Hg total pressure.

Further heating causes the wire to break. Two small spheres are seen to regress from the point at which the wire breaks. Figure 5 shows a zirconium wire burning in pure oxygen at 500 mm Hg total pressure. The speed at which these spheres regress is greatly affected by the percentage of oxygen in the atmosphere. Figure 6 illustrates the spheres in a further stage of combustion as they approach the electrodes. The atmosphere contains 60% oxygen - 40% argon at a total pressure of 50 mm Hg.

The products of combustion includes two shiny grey-black spheres which usually remain attacned to the unburned wire at the electrodes. The wire surface is generally white close to the point at which combustion has occurred. Further from this point, the wire surface is much darker. It has been noticed that this darker surface coating will flake off the wire if it is bent sharply.

Future work will include runs at pressures to 20 atmospheres. Still photos and motion pictures will be taken illustrating ignition and combustion in the various pressure regimes. Photomicrographs will be taken of the products of combustion. It is also hoped that identification of the products can be made by X-ray diffraction analysis. The effects of other atmospheres including nitrogen and carbon dioxide will also be investigated. Comparisons will be made with the work of other investigators when more detailed experiments have been completed.

The research described in the following sections include measurement of metal flame temperatures by spectrographic and two-path techniques as well as experimental and theoretical work on aluminum particle ignition.

III. Metal Flame Temperature Measurements

Little reliable data exists in the literature on the temperatures of metal flames. Glassman (4) has concluded, from thermodynamic calculations, that the temperatures of metal flames are limited by the boiling point of the oxide produced, as there is insufficient heat of reaction to vaporize all the oxide. The purpose of the present research is to test this hypothesis. If it is correct, measurement of metal flame temperature as a function of ambient pressure can yield vapor-pressure data not currently available for many refractory oxides.

Because of the high temperatures of metal flames, these temperatures must be measured optically, rather than by solid probes, thermocouples, etc. Because of the small physical dimensions of the flames of metal wires, ribbons and particles, the use of a water-cooled calorimetric probe (as used in arcjets) would alter the quantity being measured.

Because of the high luminosity of these flames, which contain light-emitting, absorbing and scattering oxide particles, line reversal temperature measurements are not applicable. Wolfhard and Parker (5) have shown that because of non-grey emission from metal flames containing micron-sized oxide particles, color temperatures differ widely from true temperatures. Because of scattering by particles, the brightness temperature does not equal the true temperature, even for an infinitely thick flame.

The technique used in the present research is a modified two-path method utilizing a background source. Light from a tungsten strip-filament lamp is imaged in the flame by a lens system. The light from the source is modulated by a chopper disc to distinguish it from the light emitted by the flame. The flame (and source) are imaged by another lens on an aperture which selects the portion of the flame to be observed. The light is chopped again at a lower frequency to permit use of AC amplifiers. A narrow wavelength region is selected by interference and dye filters, and the light is then detected by a photomultiplier.

Essentially, the absorbtivity of the flame is determined by the attenuation of the transmitted beam. The photomultiplier is calibrated in terms of brightness temperature before each run, using a tungsten lamp and optical pyrometer. Thus, the measurement of the intensity of emitted light yields the brightness temperature of the flame. By Kirchhoff's law, the absorbtivity equals the emissivity, and thus the true temperature may be computed. Using Wien's law, the following equation is easily derived; for an isothermal, nonscattering flame:

$$\frac{1}{T} = \frac{1}{T_{Br}} + \frac{\lambda}{C_2} \ln \epsilon_\lambda \quad \text{..... eq. (1)}$$

Where T is the true temperature, T_{Br} the brightness temperature at wavelength λ, C_2 is Planck's second radiation constant = ch/k, and ϵ_λ is the spectral emissivity of the flame. The wavelength of observation is chosen to avoid all emission bands and lines in

the flame spectrum, thereby avoiding the possibility of non-equilibrium radiation. The radiation observed is thus continuous emission from the oxide particles (which are at the gas temperature because of their small size).

Because of scattering by the oxide particles, the situation is not as simple as shown above in eq. (1). Also, the flame is not isothermal, and because of its small size, the temperature gradients are quite large. To correct for these effects, it was necessary to solve the equation of radiant transfer, including emission, absorbtion and isotropic scattering. The equation of transfer for a plane-parallel geometry (used to make the mathematics tractable) is (6).

$$\mu \frac{d}{d\tau} I_\nu(\tau,\mu,\nu) = I_\nu(\tau,\mu,\nu) - \mathcal{J}_\nu(\tau,\nu) \qquad \text{eq. (2)}$$

Where: $\mu = \cos\theta$

θ = angle with negative X-axis

τ = optical thickness $= \int_0^x k_\nu \rho \, dx$

ρ = density of emitters

k_ν = mass extinction coefficient at frequency ν

I_ν = monochromatic radiant intensity, $\frac{\text{ergs}}{\text{cm}^2\text{-sec - steradian-frequency interva}}$

$\mathcal{J}_\nu$ = monochromatic "source function", defined below

The "albedo for single scattering", ω_0, is defined as the fraction of the total loss from a beam due to scattering, in an infinitesimal element of length. Thus, $(1-\omega_0)$ is the fraction absorbed. It may readily be shown that

$$\varpi_0 = \frac{Qsca}{Qscat\ Qabs} = \frac{1}{1+Qabs/Osca} \quad \text{..... eq. (3a)}$$

$$1-\varpi_0 = \frac{Qabs}{Qsca + Qabs} = \frac{1}{1+Qsca/Qabs} \quad \text{..... eq. (3b)}$$

where Qsca and Qabs are the scattering and absorbtion efficiencies of the oxide particles (assumed spherical) in the flame (7).

For the radiation emitted by the flame, the source function is:

$$J_\nu = \frac{\varpi_0}{2}\int_{-1}^{1} I_\nu d\mu + (1-\varpi_0) B_\nu(T) \quad \text{eq. (4a)}$$

The first term denotes scattered light, the second term emitted light, and $B_\nu(T) = \frac{2h\nu^3}{c^2}\frac{1}{e^{h\nu/kT}-1}$, the Planck function. Since no chopper-modulated light is being generated in the flame, the source function for the modulated light from the background source is:

$$J_\nu = \frac{\varpi_0}{2}\int_{-1}^{1} I_\nu d\mu = \varpi_0 \bar{I}_\nu \quad \text{eq. (4b)}$$

Where $\bar{I}_\nu = \frac{1}{2}\int_{-1}^{1} I_\nu d\mu$

Thus, the equations of transfer to be solved, and their boundary conditions, are:

$$\mu \frac{dI_\nu}{d\tau} = I_\nu - \varpi_0 \bar{I}_\nu - (1-\varpi_0) B_\nu(T) \quad \text{eq. (5a)}$$

$$I_\nu(0, \mu<0) = 0$$
$$I_\nu(\tau_1, \mu>0) = 0$$

for the emitted light

where τ_1 is the optical thickness of the flame.

$$\mu \frac{dI_\nu}{d\tau} = I_\nu - \varpi_0 \bar{I}_\nu \quad \text{eq. (5b)}$$

$$I_\nu(0, \mu<0) = \tfrac{1}{2} F_0 \delta(\mu+1)$$
$$I_\nu(\tau_1, \mu>0) = 0$$

for the transmitted light

Fo being the flux incident from the background source and $\delta(\mu+1)$ being the Dirac delta function. (This assumes the incident flux is a collinated beam in the direction $\mu = -1$. The results obtained still apply even for beams of moderate convergence.) Solving equation (5b) formally, one finds that the term in $\bar{I}_\nu$ is small, for small values of the acceptance cone angle of the detector, and may be approximated, yielding the following result for the transmitted beam:

$$I/I_o = \frac{I_\nu(\tau_1,-1)}{I_\nu(0,-1)} \doteq e^{-\tau_1} - \frac{(1-e^{-2\tau_1})}{1+Q_{abs}/Q_{sca}} \frac{(1-\cos\theta_{max})}{2} \quad \text{eq. (6)}$$

Where θ_{max} is the half-angle of the detector acceptance cone. Even for θ_{max} as large as 10°, the second term in eq. (6) has a maximum value of .0066, and is negligible for optical thicknesses less than about 3. Thus, for optical thicknesses smaller than this, the optical thickness is given by the familiar expression:

$$I/I_o = e^{-\tau_1}$$

while for thicker flames, the connection is readily computed from eq. (6).

Returning to eq. (5a) for the light emitted by the flame, let us make the following substitutions:

$$B_\nu(T) = f(\tau) B_\nu(T_{max})$$
$$\mathcal{I}_\nu = I_\nu / B_\nu(T_{max})$$
$$\bar{\mathcal{I}}_\nu = \bar{I}_\nu / B_\nu(T_{max})$$

Where $f(\tau)$, varying between 0 and 1, describes the temperature profile in the flame, and T_{max} is the maximum temperature along any

given line of sight. The resulting non-dimensionalized equation is:

$$\mu \frac{d\Xi_\nu}{d\tau} = \Xi_\nu - \varpi_0 \bar{\Xi}_\nu - (1-\varpi_0) f(\tau) \qquad \text{eq. (6a)}$$

Formal solution of this equation yields:

$$\mu<0: \quad \Xi_\nu(\tau,\mu) = -\varpi_0 e^{\tau/\mu} \int_0^\tau e^{-\tau/\mu} \Xi_\nu \frac{d\tau}{\mu} - (1-\varpi_0) e^{\tau/\mu} \int_0^\tau e^{-\tau/\mu} f(\tau) \frac{d\tau}{\mu} \qquad \text{eq. (7a)}$$

$$\mu=0: \quad \Xi_\nu(\tau,0) = \varpi_0 \bar{\Xi}_\nu + (1-\varpi_0) f(\tau) \qquad \text{eq. (7b)}$$

$$\mu>0: \quad \Xi_\nu(\tau,\mu) = \varpi_0 e^{\tau/\mu} \int_\tau^{\tau_1} e^{-\tau/\mu} \Xi_\nu \frac{d\tau}{\mu} + (1-\varpi_0) e^{\tau/\mu} \int_\tau^{\tau_1} e^{-\tau/\mu} f(\tau) \frac{d\tau}{\mu} \qquad \text{eq. (7c)}$$

If $f(\tau)$, describing the temperature profile, is known, the second integral in eqs. (7a) and (7c) can be evaluated. $\bar{\Xi}_\nu$ however is not yet known as a function of τ. A solution could be obtained by assuming an $\bar{\Xi}_\nu$, and refining it by iteration between eqs. (7) and the definition $\bar{\Xi}_\nu = \frac{1}{2}\int_{-1}^{1} \Xi_\nu d\mu$. In the present work, it was found more convenient to utilize the Schuster-Schwartzchild approximation (8). In this approximation, the integro-differential equation (6a) is replaced by a pair of ordinary differential equations which are solved for an approximate $\bar{\Xi}_\nu$. This is then inserted in eqs. (7a) and (7c).

By expanding $f(\tau)$ in a Fourier series in the interval $(0, \tau_1)$ the integrations indicated in eqs. (7) may be performed in closed

form, and a solution obtained in terms of the Fourier Coeficients of of $f(\tau)$. The fraction of the blackbody radiation corresponding to T_{max} seen by the photomultiplier is $E_\nu(\tau_1, -1)$ which thus corresponds to an effective emissivity for the flame. Thus, in place of eq. (1), the relation between brightness temperature and T_{max} is:

$$\frac{1}{T_{max}} = \frac{1}{T_{Br}} + \frac{\lambda}{C_2} \ln E_\nu(\tau_1, -1) \qquad \text{eq. (8).}$$

By substituting various arbitrary functions for $f(\tau)$ in eqs. (7) and (8), it was found that the resultant temperature corrections were relatively insensitive to the shape of the emission profile $f(\tau)$, depending only upon its average value. Thus a sine-wave and a triangular-wave profile produced nearly identical results.

In order to estimate the shape of this profile, an apparatus was constructed as shown in Figure 7. This allows simultaneous 2-path temperature measurements along several lines of sight through the flame. By assuming a cylindrical (or spherical) flame composed of concentric isothermal zones, an analysis was performed which translates the brightness temperature and absorbtion measurements along several lines of sight into approximate temperature and emitter concentration profiles. An alternative technique would be to have a single detector rapidly and continuously scan the image of the flame along a radial line, either by means of a rotating scanning disc or an iconoscope tube. An analysis relevant to such continuous scanning was also derived. These analyses in cylindrical

and spherical geometries were made mathematically tractable only by neglecting scattering. Thus, the final solution is an iterative one between the multipath profile determination and the plane-parallel scattering conection given by eqs (7) and (8) For example, the experimental brightness temperature and absorption measurements are used to obtain an approximate temperature profile. This is inserted in eqs. (7) and (8) , which yield the value of the maximum temperature along each line of sight. These are compared with the approximate profile and used to correct it, etc.

Application of scattering corrections and an assumed temperature profile to data taken earlier on a single-aperture 2-path apparatus on magnesium ribbons burning in air at 1 atm. pressure, yielded $T_{max} = 3275^{\circ}K \pm 65^{\circ}$, in good agreement with the MgO boiling point of $3350^{\circ}K$. The uncertainty was due to variations in the literature values of the bulk emissivity, ϵ_s, of MgO, which was used in estimating the ratio of absorbtion to scattering:

$$Qabs/Qsca \approx \frac{\epsilon_s}{1-\epsilon_s}$$

Attempts have been made to measure metal flame temperatures spectroscopically by means of rotational and vibrational temperatures of AlO and MgO calculated from the band spectra of the $Al-O_2$ and $Mg-O_2$ flames. Densitometer tracings of typical flame spectra are given in Figures 8 and 9. The instrument used was a 1.5 meter Bausch and Lomb grating spectrograph, with dispersion of 15. Å/mm in first order.

As shown in the tracings, no rotational structure is resolved in the MgO spectrum, while that in the AlO spectrum is partially resolved. This difference in behavior is surprising, as the masses

and structures of the two molecules are very similar. The type of electronic transition, $^1\Sigma \rightarrow {}^1\Sigma$ is also the same, and tabulated line spacings ($\sim 1, \mathring{A}$) are similar.

Attempts were made to measure vibrational temperatures of magnesium flames burning in air at pressures from 100mm Hg to atmospheric. Magnesium was used, as longer burning times are more easily obtained and ignition more readily achieved in air for magnesium than for aluminum.

The intensity of a vibrational band is given by:

$$I = A\nu^4 P_{n'n''} e^{-E_{n'}/kT} \qquad \text{eq. (9)}$$

Where: $E_{n'}$ = vibrational energy of initial state (above the zero point energy)

I = emitted intensity

A = constant

ν = frequency of emission

n' = initial state

n'' = final state

$P_{n'n''}$ = transition probability, $n' \rightarrow n''$

$$\therefore \sum_{n''} (I/\nu^4) = A e^{-E_{n'}/kT} (P_{n'0} + P_{n'1} + P_{n'2} + \ldots)$$

$$= A e^{-E_{n'}/kT} \sum_{n''} P_{n'n''}$$

eq. (10)

Brinkman and Ornstein (9) assume initially that $\sum_{n''} P_{n'n''}$ is approximately constant for all n'. That is, the sum of transition probabilities from a given initial state to all final states is independent of the initial state. With this assumption, eq. (10) may be transformed to:

$$\ln \sum_{n''} (I/\nu^4) = \text{const.} - E_n/kT \qquad \text{eq. (11)}$$

and an approximate vibrational temperature computed. This may be inserted in eq. (9), and conected transition probabilities computed, and the solution refined by iteration.

The application of this technique requires the measurement of intensities of many bands having the same initial state, so that the summation on the right side of eq. (10) can be made. This is easily done for the AlO spectrum. However, in the flame spectrum of magnesium, only the bands for which $\Delta n = 0, \pm 1$ are visible, and only the first of these with any appreciable intensity.

However, if one ambient pressure and its associated (unknown) flame temperature T_1 are taken as a standard, and all intensities normalized with respect to it, then $\frac{1}{T_1} - \frac{1}{T}$ may be obtained as a function of pressure, without making any assumptions regarding the transition probabilities. If the hypothesis, that the metal flame temperature is very close to the boiling point of the oxide, is true, then a plot of $\ln P$ vs. $\left(\frac{1}{T_1} - \frac{1}{T}\right)$ should be a straight line of slope $\Delta H_v/R$.

Because of low plate sensitivity, the scatter in the experimental

data was too great for any such relation to be apparent. The experiment will shortly be repeated with more sensitive plates. Vibrational and rotational temperature measurements of aluminum flames will also be made.

The use of spectroscopic temperature measurements presumes the existence of thermal equilibrium between the internal modes of the molecules. However, Gaydon (10) and others have shown that lack of equilibrium may easily be detected by departures of the plotted data from linearity. Errors due to particle absorbtion will be small for bands in a small wavelength interval, as all bands will be similarly attenuated, and logarithms of intensities are plotted.

Errors may exist due to the averaging along a line of sight, and the time-averaging inherent in long photographic exposures on an unsteady flame. Coheur and Coheur (11) have reported rotational temperatures of the order of $4000^{\circ}K \pm 300^{\circ}$ for AlO in sources as diverse as exploding wires, arcs containing Al or Al_2O_3 and sparks between aluminum electrodes, at pressures ranging from atmospheric to near vacuum. The processes in the arcs are not energy-limited as are those in flames. Brinkman and Ornstein (9) have measured arc temperatures of the order of $6500^{\circ}K$ by CN band spectra. Coheur and Coheur conclude that the AlO temperature measured is simply an optimum temperature for the formation and emission of AlO. Certainly, at lower temperatures, AlO would tend to condense to Al_2O_2 or Al_2O_3, and at temperatures much in excess of $4000^{\circ}K$, dissociation to Al and O would occur. However, because of the wide experimental error in their results (a range of 600°) it is difficult to draw conclusions from them.

IV Ignition of Aluminum Particles

Metal particle ignition times and characteristics can be important in any situation in which the metal is intended to burn. Historically, much attention has been focused on aluminum. In this section a new analysis is discussed which will incorporate many more of the important variables which may influence the ignition of aluminum particles under a wide variety of experimental conditions. This analysis will be completed shortly and experimental verification will commence.

Friedman and Macek (12,13,14) studied the ignition of single aluminum particles - injected into a premixed gas flame on a flat-flame burner - by photographing the particle tracks and noting the point of ignition by the sharp increase in brightness. They reported ignition temperatures approximately that of the melting point of aluminum oxide, and ignition times of the order of tens of milliseconds. Ignition times computed on the basis of conductive ambient gas were consistent with their experimental results.

However, the condition prevailing in a regime where there are large concentrations of burning particles differ from the above experiments. A large flux of radiant energy from the burning particles can produce significant radiant heating of incoming particles. In addition, because of the distribution of particle sizes in any commerically available metal powder, larger unignited particles may find themselves surrounded by smaller burning particles, and thereby heated both radiatively

and conductively by these particles, as noted by Wood (15).

In the present work, a burner has been constructed producing a quasi-flat premixed flame of propane, O_2 and N_2, and capable of passing large concentrations of metal particles (Figures 10 11). Because of the large number, small size and close spacing of the drilled holes in the water-cooled burner plate, the individual flame cones of the premixed gas merge into a nearly flat flame with a maximum irregularity of the order of 1 mm. Since ignition distances are of the order of centimeters, to the particles, the flame is flat.

Particles are entrained into the gas stream in a mixing chamber in which tangential jets of the gas mixture impinge upon a layer of aluminum powder. The concentration of aluminum powder is determined by switching the gas streams for a known time interval from the burner to a filter which traps the particles and is later weighed. Commercially available aluminum powder is separated into relatively narrow cuts ($\approx 5\mu$ standard deviation from mean) by air elutriation. Because of heat losses to the water-cooled burner, the burned-gas temperature can be as much as 350°C below the computed adiabatic flame temperature of the mixture, and estimation of the true temperature by a heat balance on the cooling water is not accurate enough. Instead, the true temperature is measured by Na D-line reversal (with no particles in

the flame). The temperature drop can be reduced by increasing the gas stream velocity. This both decreases heat transfer to the burner and increases the mass flow, thus reducing the temperature drop.

Burned gas velocities are on the order of 500 cm/sec. Though the final particle velocity is close to the gas velocity, the particles take an appreciable distance to attain terminal velocity. Hence, experimentally measured ignition distances are converted to ignition times by integration of the equation of motion for the particle, assuming Stoke's law drag.

The theoretical analysis of particle ignition proceeded in several stages:

a) Ignition was defined as attainment of the oxide melting point, which Friedman (12,13,14) showed to be approximately the ignition temperature. First, the temperature history of an aluminum particle heated by conduction from hot ambient gases and by radiation from a plane black body at the metal flame temperature (the boiling point of the metal oxide), was studied. Radiant heat loss from the particle was also considered even where heating was purely conductive. Some typical results

of these calculations are given in the table below:

TABLE I.

Ambient Gas Temperature = 2500°K

Aluminum Particle Emissivity = .40

Particle Diameter, Microns	Calculated Ignition Time, Milliseconds: Conduction With Radiant Loss	Conduction Without Radiant Loss	Conduction and Radiant Heating With Radiant Loss
35	7.9	6.9	4.4
50	17.7	14.0	8.0
75	63.5	31.5	14.8

Thus, these calculations show that radiation, both as heat input and as loss, can be important for larger particles. Indeed, it may easily be shown that the ratio of radiative heat input (or loss) to conductive heat input is proportional to particle diameter. For particles smaller in diameter than 10 microns, the radiative contribution is negligible. Further, because of the low Reynolds number (initial Re $\approx$ 1, Final Re $\approx$ .01), conductive heat transfer has been considered rather than convective.

b) The next step was a somewhat more sophisticated model of the heating process. The cloud of burning particles radiates less intensely than a black body, unless its thickness and/or concentration are very great. The radiation from the burning cloud of particles and its dependence on concentration was computed by solving a simplified radiative heat transfer problem, subject to the grey-body assumption, and assuming that each individual burning particle radiates as a black body. The latter approximation is applicable since the radiation from each burning particle is really emitted by a dense cloud of micron-sized incandescent particles surrounding it, and the distance between burning particles is large relative to the diameter of their flame zones.

The gas temperature and velocity are not really constant, but decrease as the metal particles are heated and accelerated by the hot gas stream. Indeed, a simple heat balance shows that for any given initial gas temperature, there is a maximum concentration of metal that can be added before the gas cools below the ignition temperature and ignition does not occur. To estimate this, consider conductive heating only

$$\mu_{max}\ C_{pm}\ (T_{ig} - T_o) = (1-\mu_{max})\ C_{pg}\ (T_{go}-T_{ig}) \quad \text{..... eq. (1)}$$

$$\mu_{max} = \frac{1}{1 + \frac{C_{pm}}{C_{pg}} \left(\frac{T_{ig} - T_o}{T_{go} - T_{ig}}\right)} \quad \text{..... eq. (2)}$$

Where: μ_{max} = maximum mass fraction $\frac{\text{metal}}{\text{gas and metal}}$

C_{pm} = metal specific heat

C_{pg} = gas specific heat

T_{ig} = particle ignition temperature

T_{go} = initial hot gas temperature

T_o = initial particle temperature $\approx$ room temperature

Actually, more metal can be added than shown by eq.(2), because of radiative heating, but it has been shown experimentally that such a maximum metal concentration can exist.

The variation in gas temperature was taken into account in the computer integration of the system of differential equations describing the heating process. The cooling of the hot ambient gas (and consequent reduction of conductive particle heating) and the radiative heating of the particles have opposite effects on ignition time, as metal powder concentration is increased. In general, the net effect is to decrease the variation of ignition time with metal concentration. For some combinations of initial gas temperature, thickness of the burning particle cloud and particle emissivity, the limitation on metal particle concentration mentioned above no longer exists; i.e., in these cases radiative heating increases more rapidly than conductive heating decreases due to cooling of the gas.

c) Photographs of particle ignition on the flat-flame burner (Figures 12,13 79.μ average diameter Al particles. P=1 atm. Ug=350 cm/sec., T_{go}= 2420 ^{o}K) show that ignition occurs over a range of distances, due to the distribution of particle diameters in the sample. An average ignition distance was obtained from such photographs, both optically, and by photodensitometric scanning of the negative, and correlated with the average particle diameter (determined by photomicrography). The analysis described in b) predicted, in certain cases, that no ignition would occur under conditions where ignition was observed experimentally. This is probably due to the presence of particles smaller than the mean, which ignite first, and then conductively and radiatively heat the larger particles until they ignite.

A new analysis has therefore been made, considering the sample to be composed of a number of groups of particles, each group of one diameter, and following the history of each group. This analysis takes into account the following effects:

1. Radiative heating and heat loss
2. Conductive heating of particles by gas
3. Variable gas temperature, density and viscosity
4. Variable gas velocity
5. Conductive heating of gas by burning particles
6. Decrease in diameter of burning particles

As well as yielding ignition distances and times, this analysis will determine burning distances for each size of particle, and

the variation of intensity of the metal flame with distance (for comparison with densitometric tracings). This analysis is now being programmed for computer solution.

V. Proposed Work for the Next Report Period

Work will continue on the combustion of tantalum and zirconium over a wide range of environmental conditions of pressure and gaseous species present, as discussed in the proposal. Similar studies of calcium, and other metals will be made. Intensive efforts will be made to determine if tantalum and zirconium satisfy the vapor phase burning criteria in any environmental conditions.

The two-path metal flame temperature measurements will continue. Vibrational and rotation temperature measurements of aluminum flames will also be continued using more sensitive plates. Ignition times will be computed and compared with experimental data.

JP22-P7-1-5

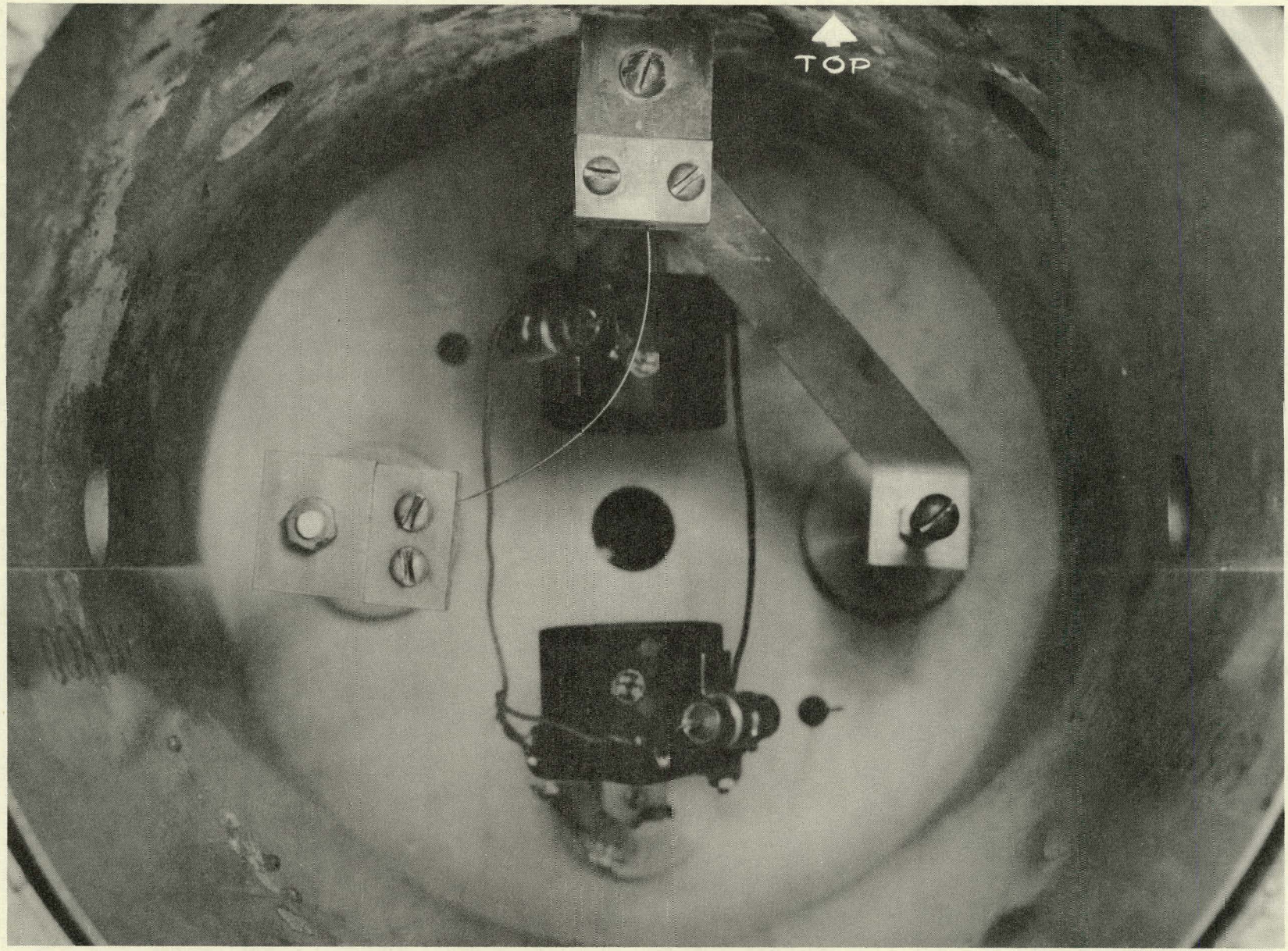

FIGURE 1

FIGURE 2

JP22-P8 5

FIGURE 3

JP22-P0 63

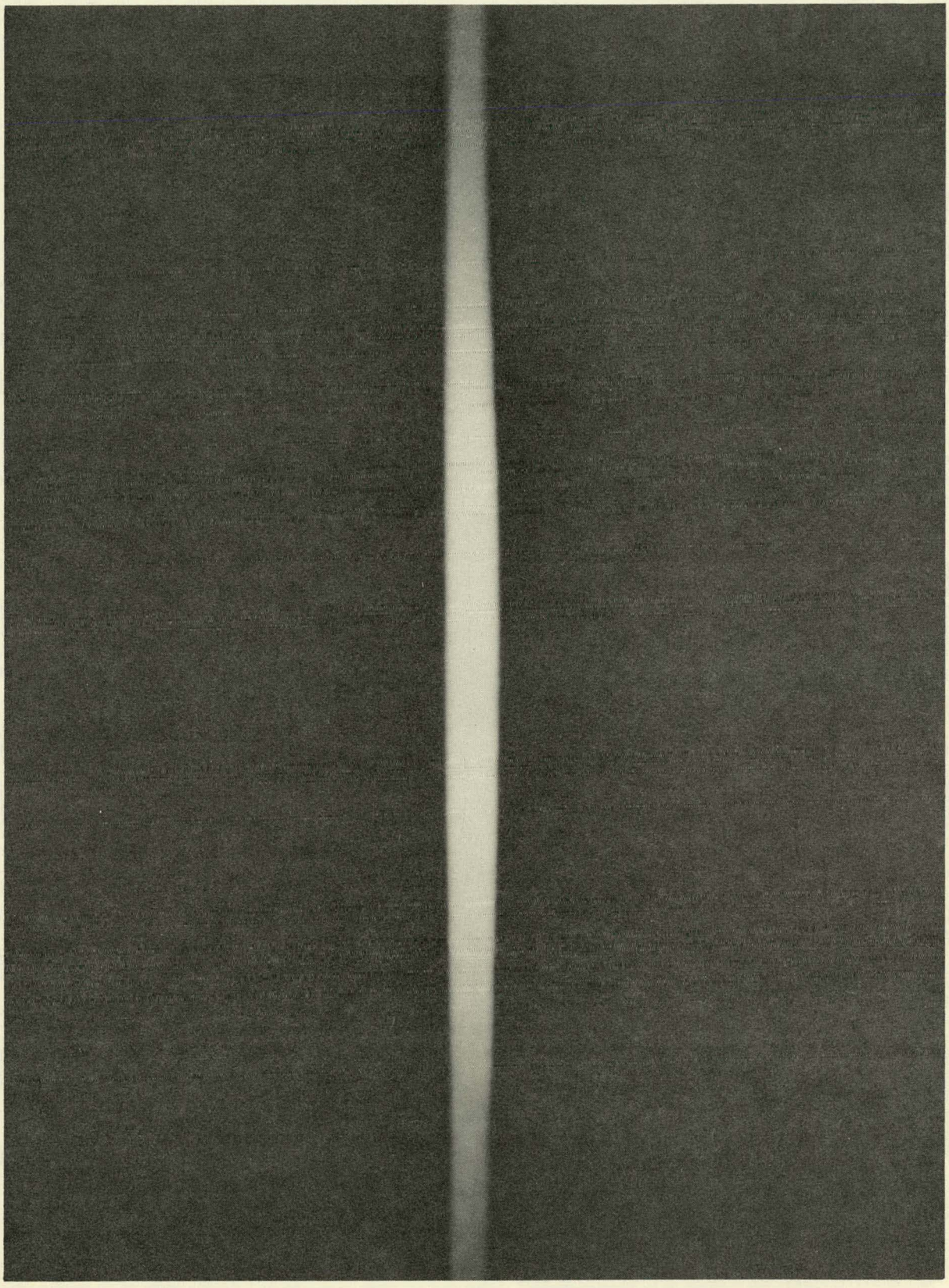

FIGURE 4

JP22-P6.

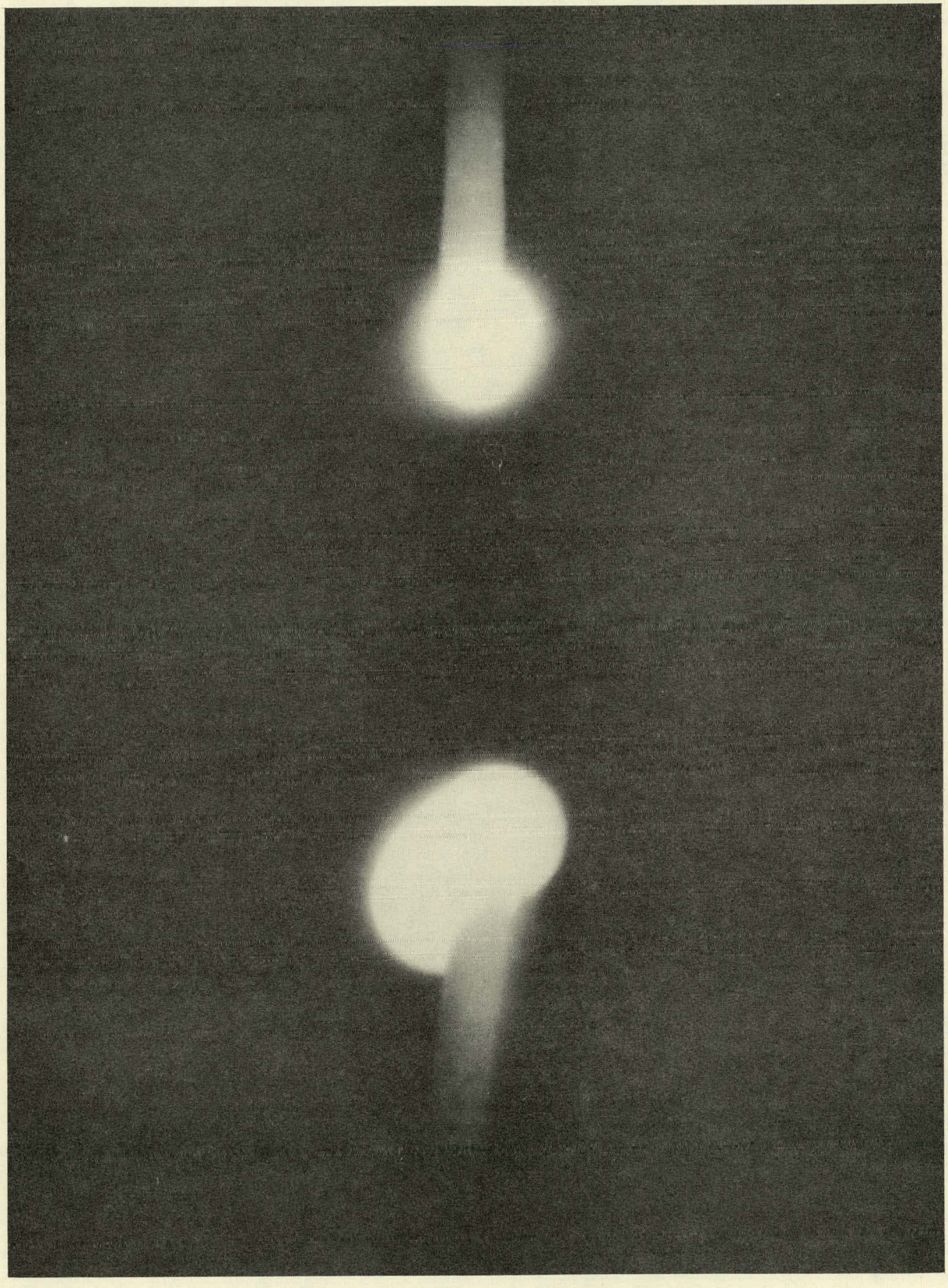

FIGURE 5

JPZZ-P5 '5

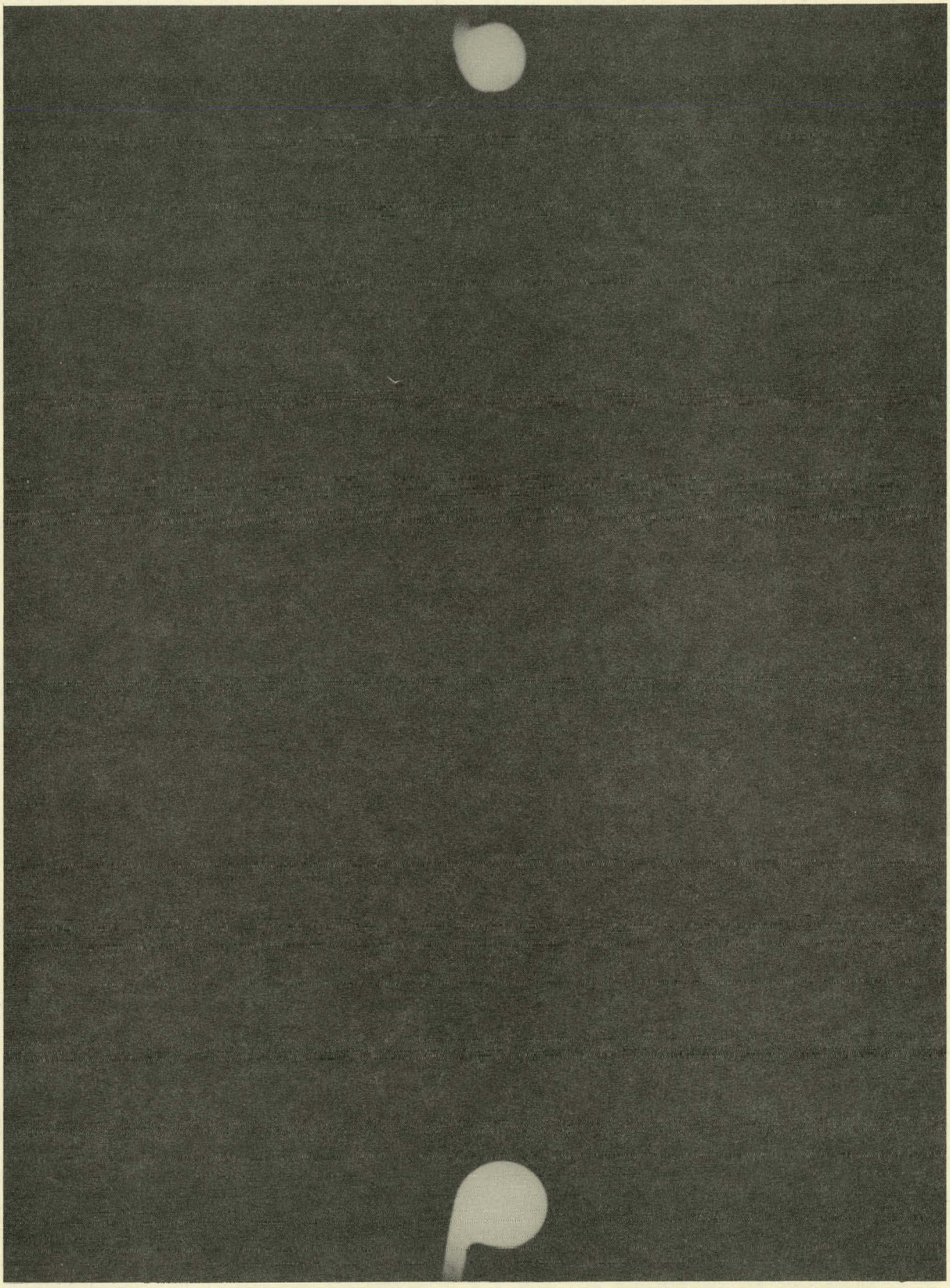

FIGURE 6

JP22- JPR 4000-65

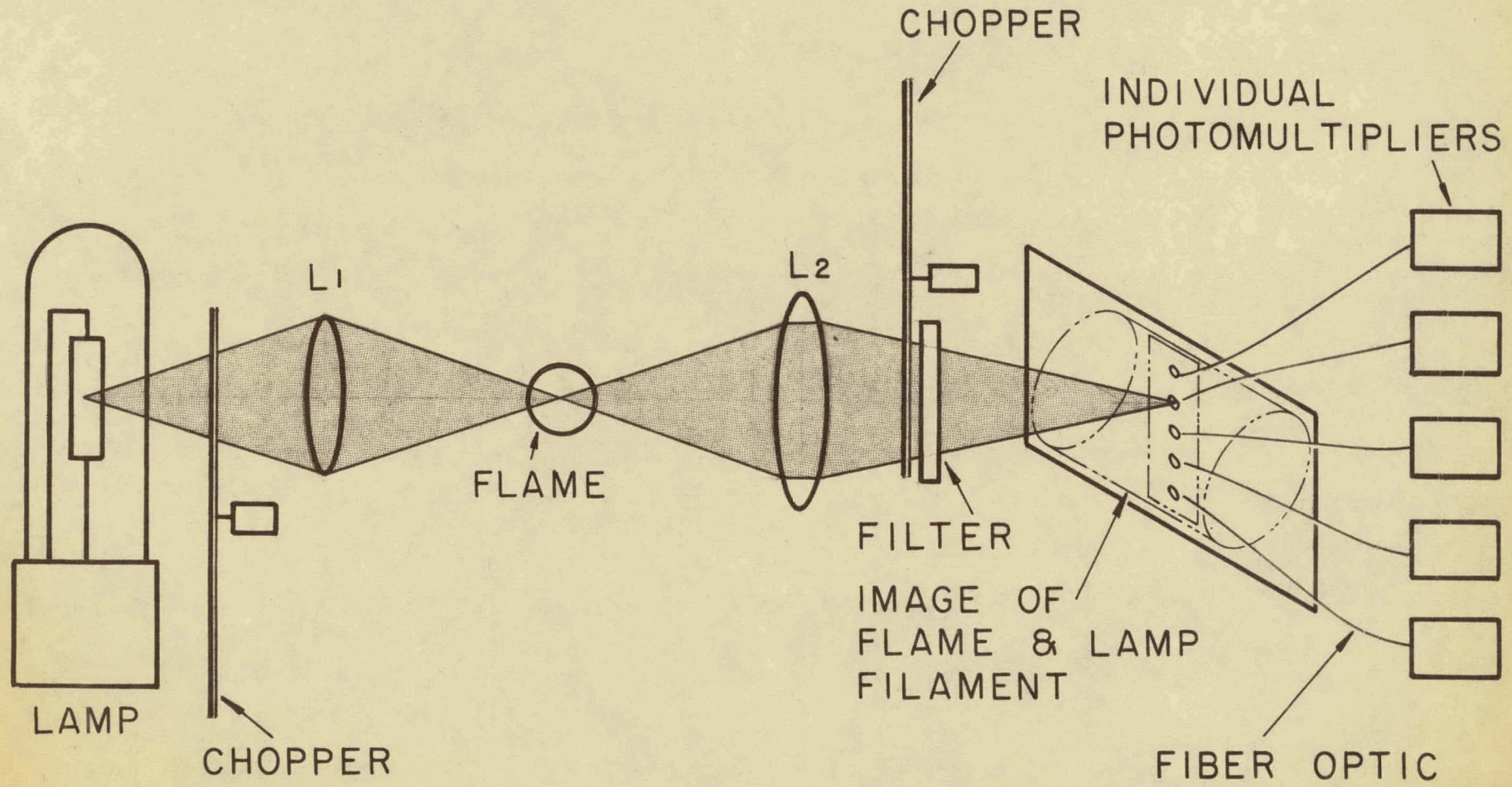

FIGURE 7

MULTI-APERTURE TWO-PATH APPARATUS

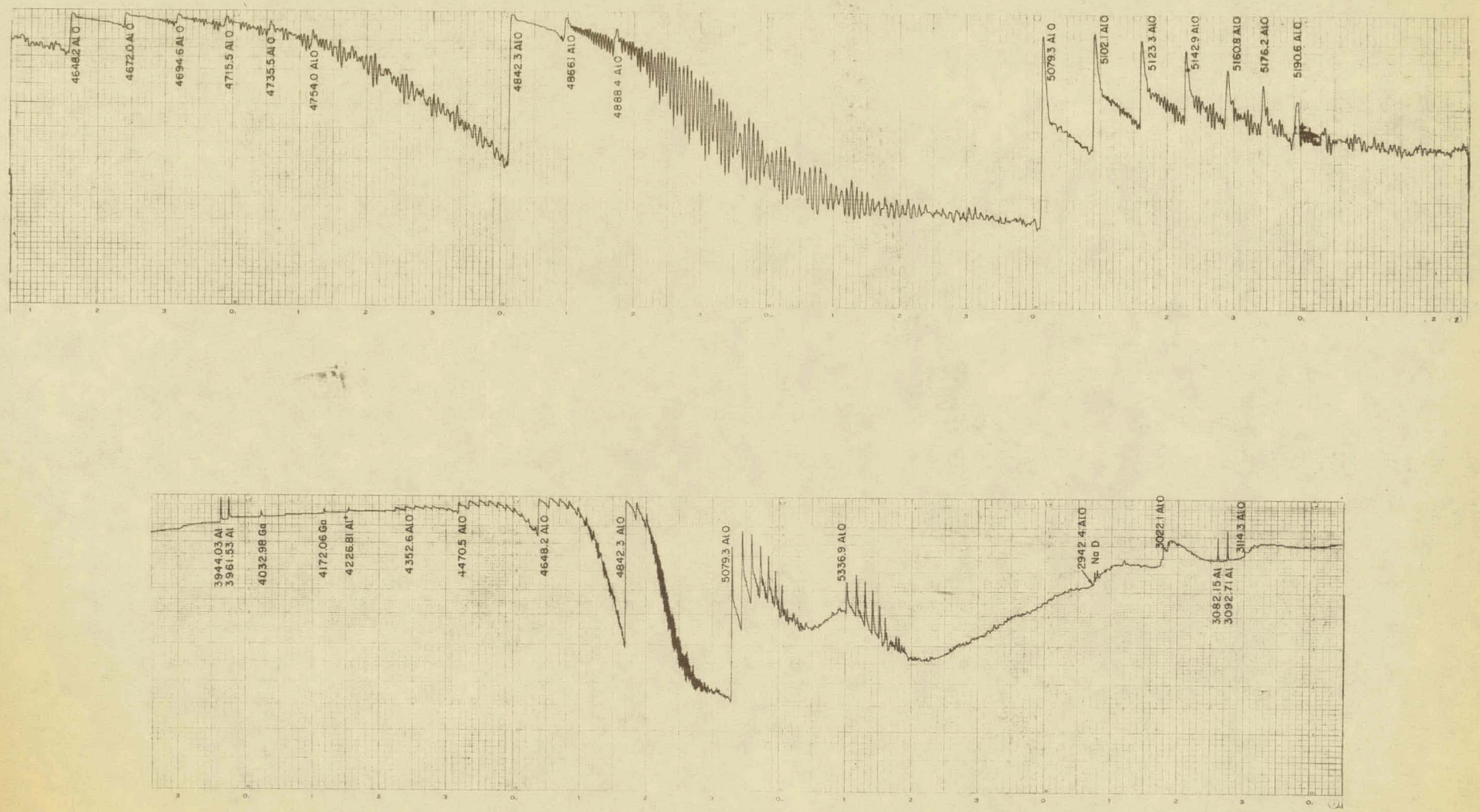

FIGURE 8

PRINCIPAL FEATURES OF THE Al-O_2 FLAME SPECTRUM

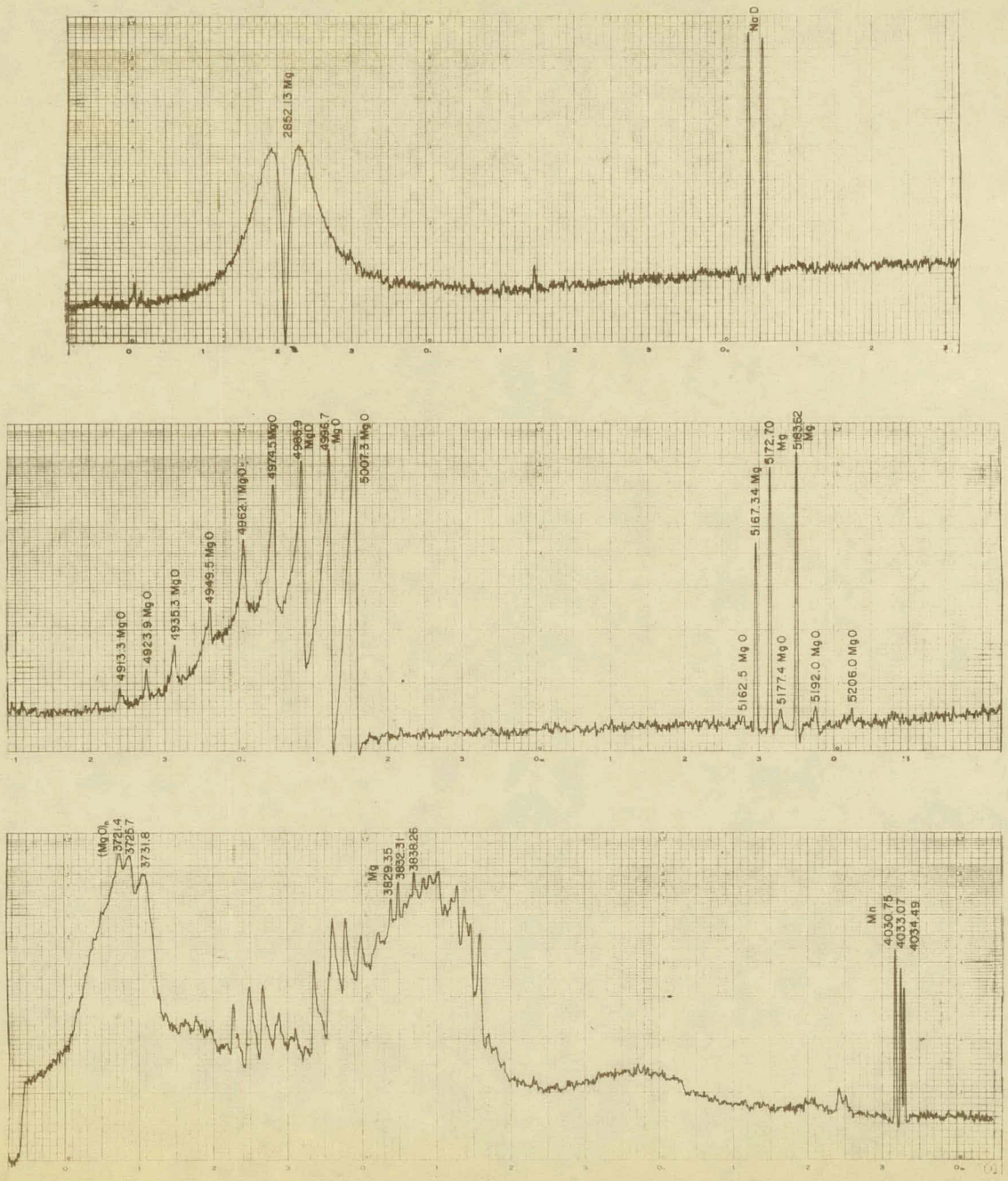

FIGURE 9

PRINCIPAL FEATURES OF THE $Mg-O_2$ FLAME SPECTRUM

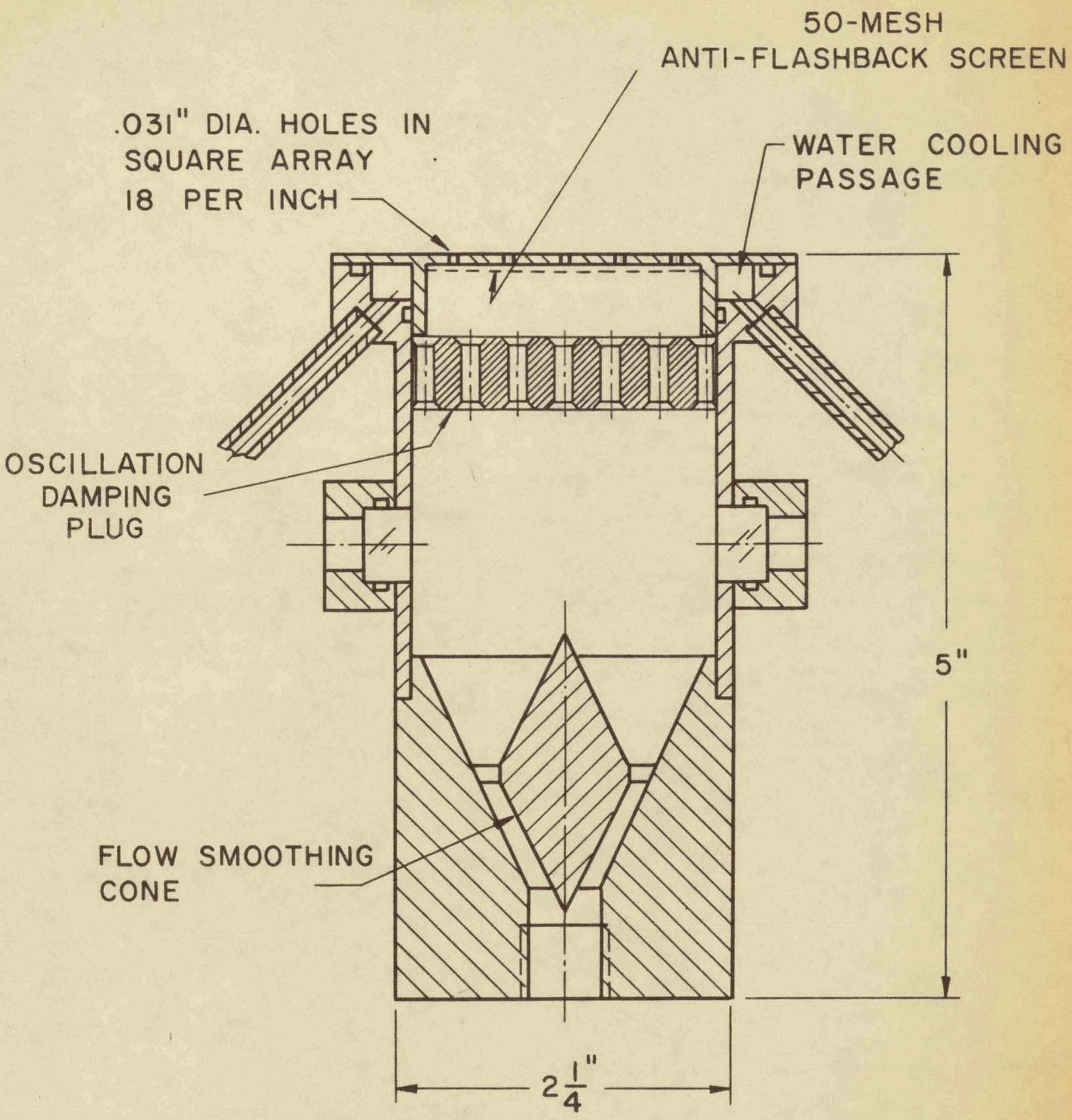

BURNER FOR GAS-METAL
PARTICLE MIXTURES

JPR 1570

FIGURE 10

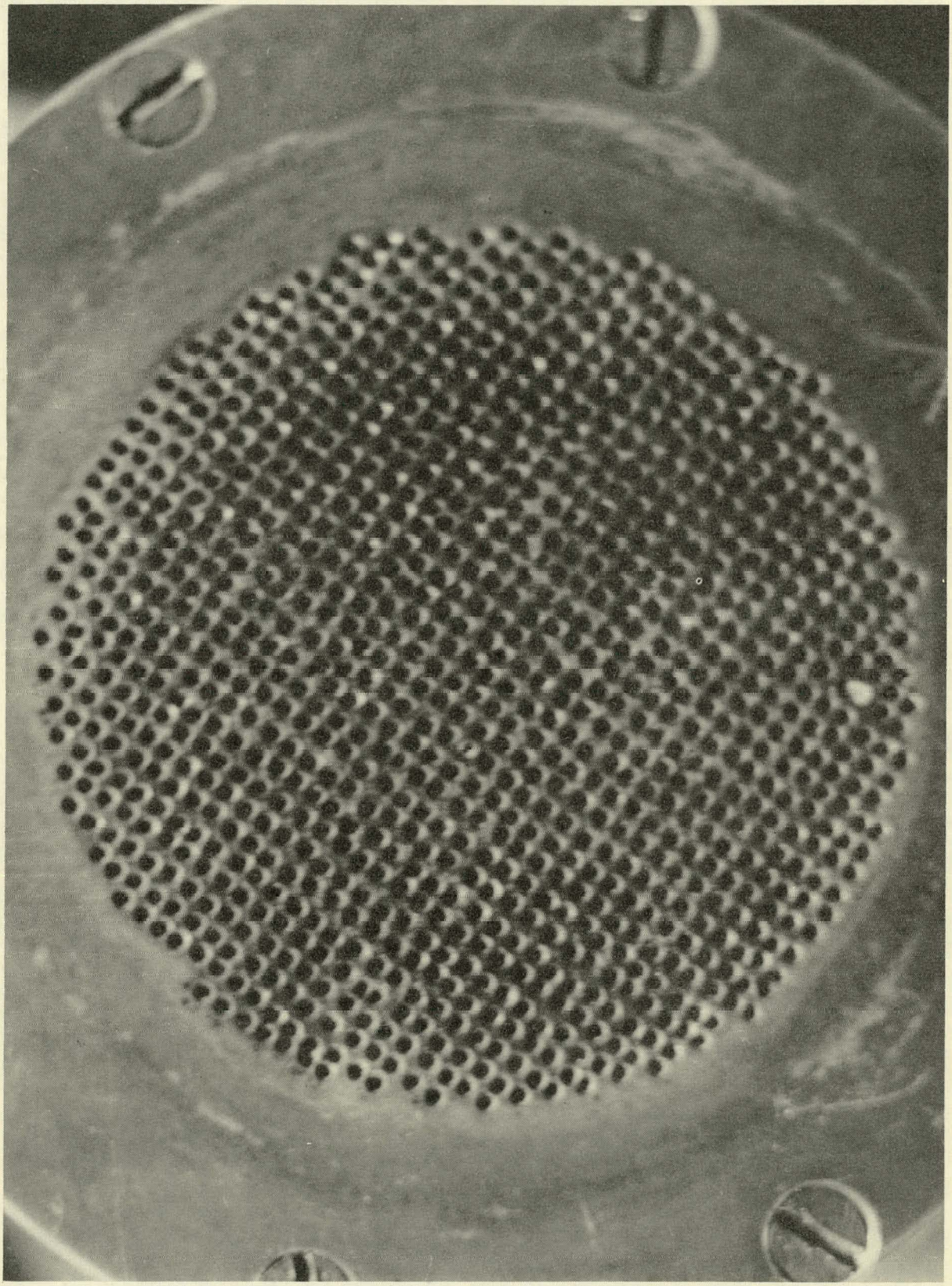

FIGURE 11

JP22-P2-65

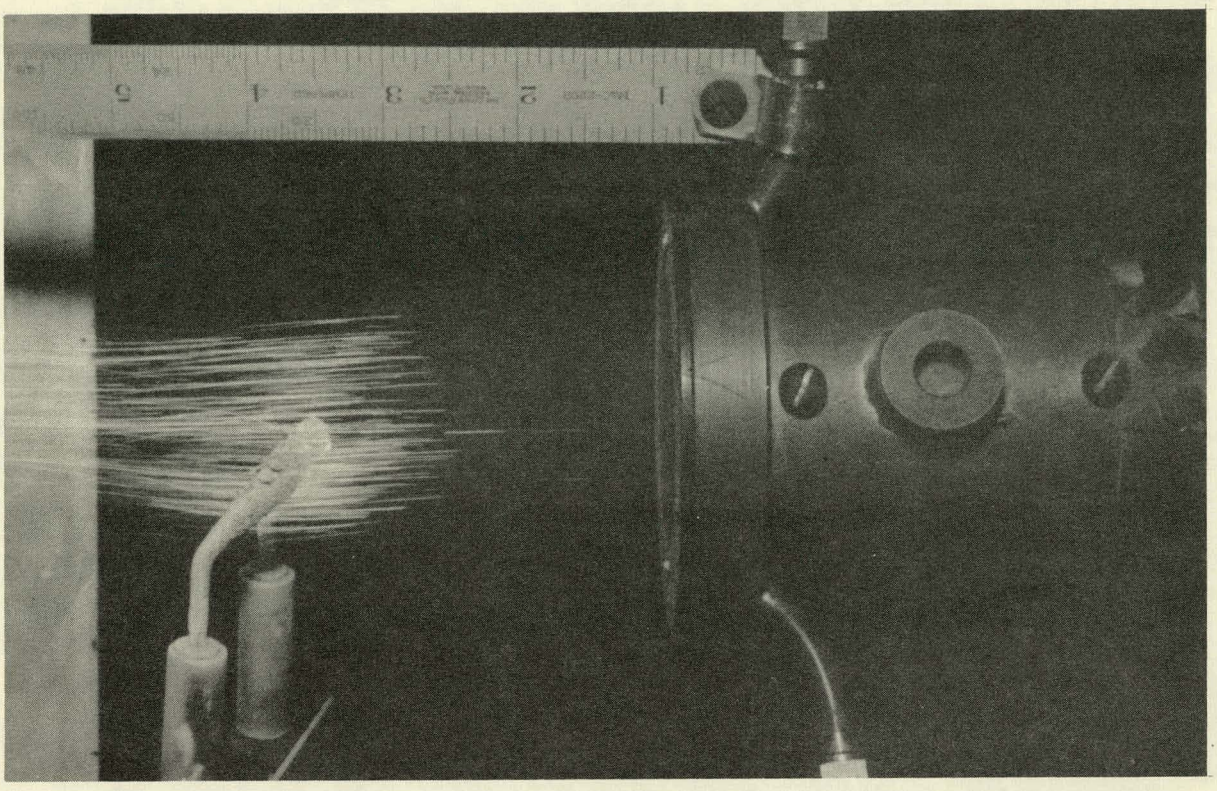

FIGURE 12

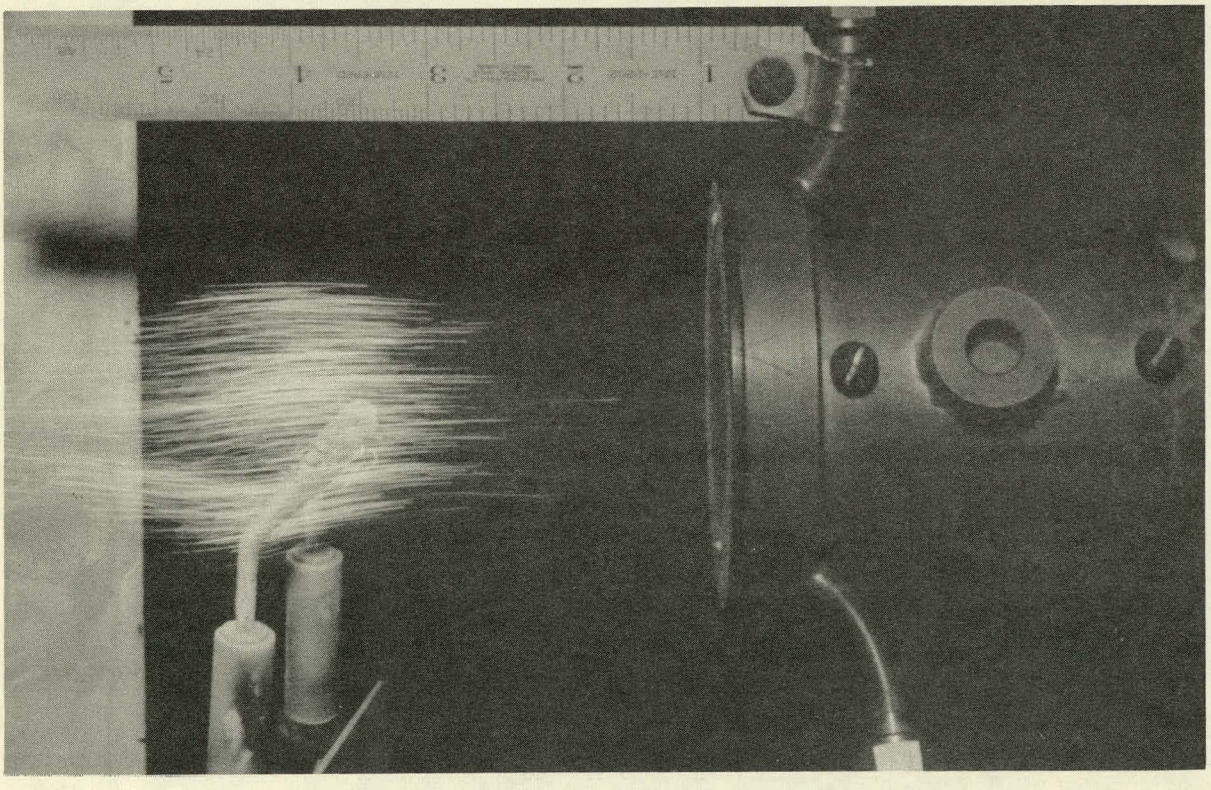

FIGURE 13